Motility of Actin Filaments on Micro-contact Printed Myosin Patterns

J. Hajne, K.L. Hanson, H. van Zalinge, D.V. Nicolau

***Abstract*— Protein molecular motors, which convert, directly and efficiently, chemical energy into motion, are excellent candidates for integration in hybrid dynamic nanodevices. To integrate and use the full potential of molecular motors in these devices, their design requires a quantitative and precise prediction of the fundamental mechanical and physicochemical features of cytoskeletal proteins operating in artificial environments. In that regard, the behavior of protein molecular motors constructs in/on nano-confined spaces or nanostructured surfaces that aim to control their motility is of critical interest. Here, we used a standard gliding motility assay to study the actin filaments sliding on a surface comprising heavy mero myosin (HMM) micro- and nano-patterns. To print HMM, we used negative tone, micro contact printing of a blocking protein (Bovine Serum Albumin, BSA) on a nitrocellulose surface, followed by specific adsorption of HMM on BSA-free surfaces. While the large BSA-free patterns allowed for selective confinement of actin filaments motility, the BSA-stamped areas displayed intricate nano-sized HMM patterns, which enabled a deeper analysis of the nano-mechanics of actomyosin motility in confined spaces.**

***Index Terms*— actin filament, actomyosin, micro contact printing, molecular motors**

I. Introduction

Protein molecular motors are excellent examples of natural devices, which operate with remarkable energetic efficiency and accuracy compared to human made devices. Biological motors also apply various sources of chemical energy to produce their motion such as hydrolysis of ATP [1] or gradient of ions.[2, 3] Some of the most notable examples of these dynamic nanodevices include: rotary motors, such as the F_oF_1-ATP synthase [4-6] or the bacterial flagellar motor;[7, 8] and linear motors, comprising the super family members of kinesin,[9, 10] dynein [11] and myosin proteins,[12, 13] which move in a step-by-step fashion along the tracks formed of cytoskeletal filaments.[3, 14, 15]

Protein molecular motors are excellent candidates for the integration in dynamic nanodevices, for various applications,[3, 14-18] as they offer important advantages: high energetic efficiency, which derives from the direct conversion of chemical energy into motion;[15] operation independent of external power, as their fuel (ATP) is extracted from surrounding fluid;[19] reduced physical size [15, 19, 20] opening large multiplexing opportunities and continuous operation, making them ideal candidates for cargo manipulation applications.[3, 17]

A critical operational element of molecular motors-based dynamic nanodevices is the control of the motion and directionality of cytoskeletal filaments, which can be achieved based on their inherent polarity,[15, 19, 21] but more often in planar gliding devices with various external techniques.[19] The control of motility ensures that molecular motors-based nanodevices can complete complex tasks such as biocomputation,[22] energy transduction,[23] or biosensing.[24-28]

Among several methodologies for achieving the confinement and guidance of the motor-propelled cytoskeleton filaments, the selective patterning of motor proteins on planar surfaces on which the cytoskeleton filaments move is the most straightforward. However, the outcome of the patterning of proteins is difficult to predict, due to extremely complex interactions of proteins with surfaces, which, despite decades of intense research, eluded reliable, engineering level predictions.[29] Because of the extreme sensitivity of motor proteins, the patterning derived from standard techniques [30-33] could be replaced by soft-lithography, which is less expensive and more suitable for protein applications [15, 34] as the protein is applied directly on the surface of an elastomeric stamp and then transferred to a substrate.[15] Patterning motor proteins by using microcontact printing has been already demonstrated by Kolli *et al.* [35] who printed poly (amidoamine) (PAMAM) dendrimers on a glass surface. As PAMAM dendrimers support actomyosin motility, the motion of actin filaments can be successfully confined to predefined tracks.[35]

Another critical design element of molecular motors-based dynamic nanodevices is the dimensions of the micro- or nano-structures able to confine the motility of cytoskeletal

This paper was submitted for review on @@@. The work presented here was financially supported by the European Union Seventh Framework Programme (FP7/2007-2011) under grant agreement number 228971 (MONAD) and Defense Advanced Research Projects Agency (DARPA) under grant agreement N66001-03-1-8913.

J. Hajne and H.van Zalinge are at the University of Liverpool, Department of Electrical Engineering and Electronics, Brownlow Hill, Liverpool, L69 3GJ, UK.

D.V. Nicolau was at the University of Liverpool, Department of Electrical Engineering and Electronics, Brownlow Hill, Liverpool, L69 3GJ, UK; and the Industrial Research Institute Swinburne, Swinburne University of Technology, Hawthorn, Vic 3122, Australia. He is now at McGill University, Department of Bioengineering, Faculty of Engineering, Montreal, Quebec, H3A 0C3, Canada (email: dan.nicolau@mcgill.ca)

K.L. Hanson is at the Industrial Research Institute Swinburne, Swinburne University of Technology, PO Box 218 Hawthorn, Vic 3122, Australia.

filaments. A large number of reports, periodically reviewed,[36] address this challenge, but unless complex nanofabrication is used to produce structures that confine the movement of cytoskeletal filaments in hollow tubes,[37] effective motility control is difficult to achieve in channels which are covered by motor proteins not only on their floor, but on their walls as well. Another critical design problem is to be able to predict not only the lateral dimensions of confining structures, e.g., channels, but also their allowable radius of bending, which, in concert with the persistence length of the motile cytoskeletal filament, will preclude its escape from the designed trajectory.

To this end, topographically flat micro-geometries of HMM have been fabricated by the micro contact printing of bovine serum albumin (BSA), followed by HMM immobilization on the BSA-free surfaces. Interestingly, the non-homogenous stamping of BSA offered the opportunity of observing the motility of actin filaments on flat, tortuous, nanometer-level HMM-functionalized trajectories. The tracking of actin filaments with high accuracy in tightly confined spaces allowed a nanomechanical analysis. This allows for an improved prediction on how the actin filaments will behave in tightly confined geometries essential in making the devices smaller.

II. Methods and Materials

A. Protein Preparation

We extracted and purified myosin and G-actin from the rabbit skeletal back muscle using previously reported methods.[38-41] Heavy meromyosin (HMM) was prepared by proteolytic cleavage of myosin (20 mg/mL in 0.5 M KCl, 50 mM KPO4 pH 6.5) with 0.07 mg/mL α-chymotrypsin. Prior to use in motility studies, G-actin was dissolved in 1mM DTT to a concentration of 2 mg/mL and clarified by centrifugation (40000 rpm for 60 min). F-actin was simultaneously polymerized and fluorescently labeled by incubation of equal molar quantities of G-actin and AlexaFluor® 488 Phalloidin (Molecular Probes) in 4 mM imidazole pH 7, 2 mM MgCl2, 0.1 mM EGTA, 3 mM NaN3 and 1 mM DTT.

B. Polymer Surface Coating

Super clean nitrocellulose (NC) was purchased from Ernest F. Fullam, Inc. (Latham, NY). Glass cover slips were cleaned by sonication in 70% ethanol, dried in a stream of N_2, and spin-coated with NC (1% w: v in amyl acetate) at 3600 rpm.

C. Protein Patterning

Microstructures used for the micro contact printing were fabricated from poly(dimethylsiloxane) (PDMS; Sylgard 184, Dow Corning). A positive-relief silicon master was fabricated by standard photolithography techniques followed by deep reactive-ion etching.[42] The negative-relief PDMS replica was then made by casting and curing the degassed PDMS prepolymer and curing the agent mixture (10:1 by weight) using well-established procedures.[43] The patterned PDMS surface was rendered hydrophilic by deep UV exposure, and micro structures were capped by sealing to a thin layer of unpatterned PDMS (spin-coated on a glass). Bovine Serum Albumin (BSA) labeled with Rhodamine (2 mg/mL in PBS 10 mM, Molecular Probes) was diluted with 10 mM PBS to the concentration of 50 µg/ mL; and adsorbed immediately over a freshly prepared PDMS stamp (~100 µL) for 40 minutes. The stamp was rinsed subsequently with PBS 10 mM (3x 100 mL) and then with MilliQ water (3x 100 mL). Subsequently, it was air dried and immediately stamped over a cleaned glass cover slip. We allowed conformal contact to occur spontaneously, and finally at room temperature we carried out stamping for 60 seconds without the use of additional pressure.

D. Motility Assays

We modified actomyosin motility assay procedures from Sellers *et al.*[44] The motility flow cells were constructed by sealing two parallel edges of the BSA-patterned cover slip to a standard glass microscope slide using double-sided tape (100µm thickness) as a spacer. Heavy meromyosin, HMM, was diluted to 0.1 mg/mL in 10 mM MOPS pH 7.2, 20 mM KCl, 5 mM $MgCl_2$, 0.1 mM EGTA, 10 mM DTT (Buffer A), introduced into the flow cell and allowed to attach on the surface for 2 minutes. The cell was then flushed sequentially with the following (all in Buffer A): (a) 1 mg/mL BSA, (b) 5µM unlabeled F-actin, (c) 1.5 mM MgATP, and (d) 5 nM labeled actin. The motility was initiated by the addition of 1 mM MgATP in Buffer A. A photobleaching inhibition cocktail, consisting of 2.5 mg/mL glucose, 0.1 mg/mL glucose oxidase (Sigma G-7016) and 0.02 mg/mL catalase (Sigma C-100), was also added. The set-up of the experiment, with examples of the trajectories of actin filaments over the

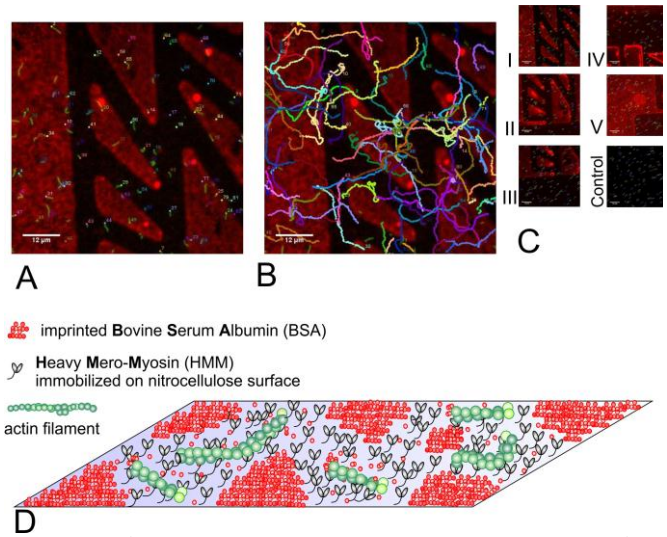

Fig 1. Actin filaments sliding on myosin motors. (A, C) Snapshots of the actin filaments movement on micro-imprinted surfaces in various geometries taken from 6 different experiments (I-V, and Control). Both actin filaments (green) and BSA (Bovine Serum Albumin) stamps (red) are fluorescently labeled. (B) Examples of the trajectories of actin filaments correspond to assay I. Both actin filaments and BSA areas are fluorescently labeled. (D) Schematic view of actin filaments moving on HMM heads. The movement takes place also within imprinted BSA molecules that block attachment of myosin motors to the nitrocellulose surface.

patterned BSA/HMM surface is presented in Figure 1.

E. Measurement of the Surface Density of Adsorbed HMM

The measurements of the amount of HMM adsorbed on model surfaces used an in-house built Quartz Crystal Microbalance (QCM) system. The QCM system integrated the quartz resonators into an oscillator circuit, and comprised a Phase Lock Oscillator (PLO-10 from Inficon) integrated with a PC equipped with a counter/timer PCI card, controlled by a custom interface built with LabView (V7.1, National Instruments, Austin TX). The system used 5 MHz AT-cut, gold coated, quartz crystals. The PLO-10 Phase Lock Oscillator also provided a DC output voltage that was inversely proportional to crystal motional resistance. Crystal resonant frequency and motional resistance were monitored continuously and recorded every 2 sec. The surface density of motor protein (HMM) adsorbed on a nitrocellulose surface (NC) has been estimated at 1465 molecules/μm^2.

F. Image Acquisition

The motility experiments were observed, at room temperature (23-25 ºC), on an inverted microscope (Olympus IX71) using a PlanApo 100x oil objective (Olympus), epifluorescence optics (FITC filter set), and mercury light source. A Coolview FDI high-resolution camera (Photonics Science Ltd.) recorded images every 150 msec for 60 sec. The camera worked with Image-Pro Plus software (Ver. 5.0, Media Cybernetics).

G. Image Storage and Pre-processing

The recorded images were stored as uncompressed (8-bit) tiff movie files consisting of two independent channels: one designated for actin filaments and the other one used for imaging of BSA stamps. Preliminary image processing was performed separately for: experiment visualization; motility analysis, and quantification of fluorescence used to calculate the local fluorophore concentration. For visualization purposes, movies stored as tiff files were converted into RGB composite files. Subsequently, the autofluorescence background was removed, the contrast was enhanced (using 'Enhance Contrast', with saturated pixels value set as 0.4%), adjusted brightness interactively (using 'B&C tool'), and finally the images were smoothed (using 'Smooth' function). All mentioned operations used standard algorithms in ImageJ environment. To analyze motility, the channels were split and only the channel with recorded filaments was chosen for further analysis. The images were thresholded using 'Otsu' algorithm available in ImageJ. Consequently, by thresholding operation, all images in the stack were made binary, so that the filaments could be tracked with MTrack2 plugin that is based on a particle filter (see 'Spatio-temporal Data Analysis' in Methods section below for further information). Finally, in order to optimize images for the quantitative analysis of fluorescence, the raw files were processed by using functions which enhance picture quality, but do not alter relative pixel values at the same time. Firstly, we applied ImageJ command 'Enhance contrast' (at pixel saturation 0.4%, without checking the normalization or histogram equalization boxes). The brightness and the contrast were adjusted interactively by using ImageJ B&C tool. The pre-processed images of the BSA stamps were further analyzed with MATLAB tools (see 'Fluorescence intensity analysis' below and Supporting Information for the commands used).

H. Persistence Length Measurements

We determined persistence lengths of the filaments by using methods described elsewhere.[45-51] The measured values of the contour lengths L, as well as averaged end-to-end distances <R> yielding free ends of the filaments, were taken from 100 consecutive frames for every filament, and consequently used to estimate persistence length Lp (Figure 2). This was achieved by using the MATLAB solver available in MuPAD®. We determined the persistence length, Lp, from equation (1) (by Landau and Lifshitz) [21, 51, 52] given below:

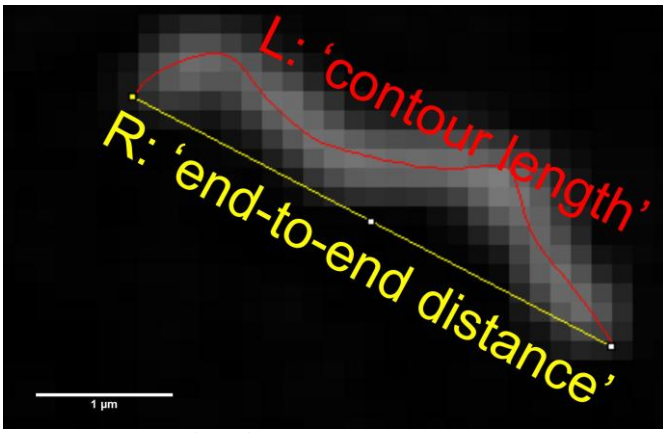

Fig 2. Illustration of the filament contour L and end-to-end distance R needed for determination of persistence length Lp. The 'spline' function in ImageJ was used to select the contour of the filament.

$$\left\langle R^2 \right\rangle = 2 \cdot L_P^2 \cdot \left(\frac{1}{e^{L/L_P}} + \frac{L}{L_P} - 1 \right) \qquad (1)$$

I. Spatio-temporal Data Analysis

The object tracking features of ImageJ were used to determine the coordinates of both the centroid and the head positions of the filaments. The centroid positions were analyzed with MTrack2 plugin based on particle analyzer; while the head positions were tracked semi-automatically with MTrackJ plugin. The coordinates from consecutive frames were used to derive the motility statistics. The following software was used to obtain the statistics of actin filaments: (i) Minitab® version 16.2.2 (descriptive statistics [53-55]); (ii) MATLAB® version 7.12.0.635 (R2011a) (taking pixel intensity values and image analysis according to the methods described by Gonzalez *et al.*[56] see also Supporting

Information), S-PLUS® 8.0 for Windows, Insightful Corp. (used for permutation tests according to the methods given by Moore *et al.*[54]), and OriginPro 8.5.0 SRO (plotting frequency counts [53]). The step velocity was calculated as the distance travelled by the filament head/center of mass divided by the time between sampled frames. The acceleration was calculated as the difference between the two consecutive velocities divided by the time between two consecutive frames. The deflection angle was calculated for each combination of the three consecutive points as the difference between (i) the direction of filament head movement between two consecutive points; and (ii) the direction of filament head movement between the next two consecutive points. The absolute value of the directional difference was calculated such that the angle of the directional change was always less than 180° (See also Supporting Information).

J. Fluorescence Intensity Analysis

The information on intensity values of individual pixels was used to quantify the fluorescence intensity. By using the known number of randomly distributed HMM molecules on a nitrocellulose (NC) surface, as measured above, the pixel intensities were calibrated to the estimated number of myosin heads per μm^2. Because BSA is blocking the access and thus the attachment of myosin onto the surface, the level of red fluorescence, which quantifies the surface concentration of BSA, is anticorrelated with the number of myosin heads. The density of HMM molecules on a BSA-free surface (seen as black regions in Figure 1 and subsequent Figures), measured using QCM method, was estimated at 2930 myosin heads/μm^2. To compare the amount of BSA between different motility assays, the area under each plot has been calculated with OriginPro8.5 and given in arbitrary units [a.u.]. However, it should be noted that the values presented here are best estimations as, despite the high quantum efficiency of the optical system, it is never possible to get a perfectly linear result out of any camera. More elaborate information on the topic is available in a number of publications.[57-63] A full description of the calibration is presented in the Supplementary Information. Figure 3 presents the probability of an actin filament moving in a particular direction.

K. Motility Statistics

The object-specific measurements included various parameters of actin motility, i.e., velocity, acceleration, intensity of visited pixels and deflection angles. As none of these parameters displayed a normal distribution, to characterize results statistically, median values were used to determine the central tendency (instead of mean values that are conventionally used for normally distributed data). Additionally, the following statistical measures were calculated: the minimum, 25% quartile, 75% quartile, and the maximum value of each parameter to characterize the data spread (instead of giving standard deviations used commonly for normal distribution characterization). The filament head

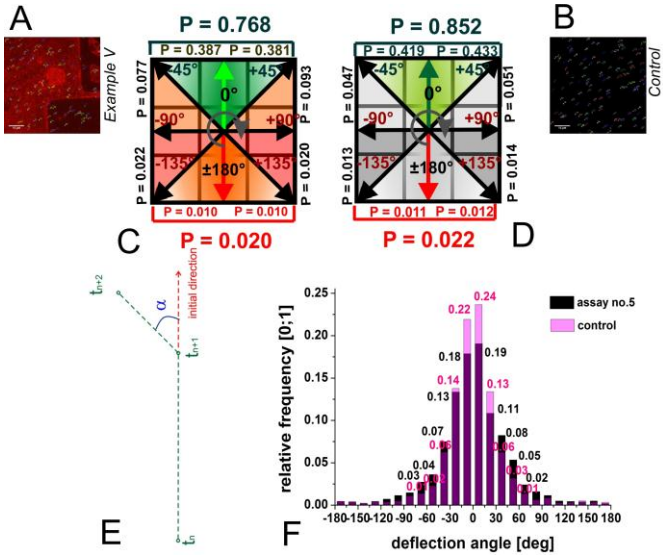

Fig 3. Probability of approaching a particular area by the filament head. The probability that a filament head will move into a particular direction is estimated from measurements of deflection angles for different actin filaments (Fig. A) and Control Assay (Fig. B). According to assumptions, a hypothetical filament tip is situated in the middle of a 9-pixel square (Figures C and D). The deflection angle indicates the change of directionality (Fig. E). The frequency counts of the measured deflection angles show that both the amount and the geometry of BSA on a surface affect the directionality of the filament movement (Fig. F).

and the filament centroid (XY) positions were analyzed statistically and compared (see 'Part II. Statistical Description and Comparisons' in Supplementary Information).

To specify the significance of differences in the mean values between parameters for various myosin patterns,

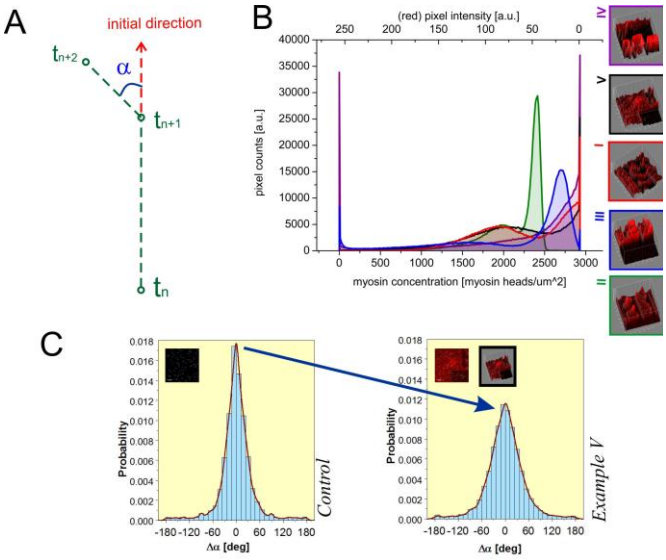

Fig 4. Assessing the amount of BSA imprinted on a surface via measuring pixel intensity values. (A) Illustration of deflection angle definition. (B) Red pixel intensity values (top X-axis) were translated into the number of myosin heads per μm2 (bottom X-axis). Pixels having particular value are counted (Y-axis) and plotted in order to assess the relative amount of BSA between different motility assays. The area under each plot is calculated. (C) Deflection angles are indicated as Δα on the X-axis, whereat probability values [0, 1] are given on the Y-axis. Area under each of the density curves is equal 1. Histograms with the probability density curves show that there is a link between the amount of imprinted BSA and directionality of the filament movement. Probability that the filament tip will deflect from its original direction increases when BSA is applied (Example V).

permutation t-tests were used (see Figures 4A, B, and C given in Part I of the Supplementary Information). Detailed description of the theory and the practical applications of permutation tests are given by Moore *et al.*[54] 6752 values of each parameter were bootstrap-sampled (with the number of replications equal 2000). The values were taken from the motility data obtained for different myosin patterns. In agreement with the central limit-theorem, the two distributions of the means were always normal and thus could be analyzed for differences using Welch Modified Two-Sample *t*-Test (two-sided) statistics.

L. *Histograms and Density Curves*

We cantered histogram bins and added corresponding density curves by using the kernel density estimator available in S-Plus® version 8.0. Detailed description of the method provided by the software is described by Carmona *et al.*[64] We set the number of bars at 26 and the number of output points as 10000.

III. RESULTS AND DISCUSSION

A. *Microcontact Printing of BSA and HMM*

The microcontact printing of BSA results in two types of patterns: larger, micrometer-sized features conforming to the designed patterns on the PDMS stamp; and smaller, submicron-sized, tortuous features (Figure 1A, red areas). The existence of finely printed features, albeit accidental, can be explained by the extraordinary resolution capability of the micro-contact printing, reported to be down to single molecules.[15] However, because the gravity, adhesion, and capillary forces are critical when the elastomeric stamp is applied, some of the features to be imprinted on a surface may collapse or distort.[65] Moreover, the amount of protein obtained on the stamp is dependent on the duration of inking and protein concentration in prepared solution,[15] therefore, regulating the pressure, the printing time, and the concentration of protein in solution [66] are non-trivial problems, difficult to control.

Subsequent to BSA patterning, HMM protein preferentially adsorbs to the BSA-free regions (Figure 1A, dark regions). This propensity of specific adsorption is revealed by the confinement of the filaments motility. Measured values fall into the entire intensity range, given in arbitrary units, that varies between 0, i.e., no BSA present (or undetectable) and hence maximum HMM present, to 255 [a.u.], i.e., maximum BSA present, or rather no HMM present. In ~50% of events the filaments visit pixels with intensities that are below 65 [a.u.]. Furthermore, in ~75% of all cases, the measured pixel values are below 106 [a.u.]. Because fluorescent intensity relatively quantifies BSA concentration, the pixel intensity values can be consequently translated into estimated concentrations of myosin heads per unit area (this calibration curve is shown in the supplementary information). Therefore, within 75% probability, the actin filaments are not able to translocate if the concentration of myosin heads decreases below the threshold value of 1712 myosin heads per μm^2. This result is in a good agreement with the values reported by others.[21] Moreover, these conclusions are based on the image analysis of the large number of independent events, i.e., 43572, and involves actin polymers of the lengths between 0.1 and 2.77 μm.

B. *Analysis of Motility in Tightly-Confined Space*

The size of the pixel is determined by the optical resolution of the microscope used. In the present study, the pixel size is approximately 175 nm. At the median velocity of actin filaments, i.e., 2 μm/s, or 300 nm/150 msec (frame rate), the head visits each pixel per frame. Even the rare instances of filaments moving with higher velocity, i.e., the maximum 3 μm/s, will still result in the head of the actin filaments visiting, most of the time, one pixel per frame, i.e., 12 pixels in 10 frames.

The analysis of the angular changes of the movement of actin filaments on myosin-functionalized surfaces, which has been studied theoretically,[16, 67, 68] was used previously to assess the function of molecular motors on surfaces [69] or at the border between two different surfaces.[70]

The histograms of the deflection angles with the probability density curves (Figure 4) revealed that there is a strong statistical link between the amount of imprinted BSA, or conversely the density of HMM, and the directionality of filament movement. Indeed, statistical measurements of actin filaments motility show that the relative area of the stamp and the amount of imprinted BSA protein are strongly correlated with the overall angular deflection of the actin filaments. Indeed, the probability of a significant deflection (above ~30°) of the head of the filament from its original direction (Figures 3C, 3D, 3F) increases as the area and the density of HMM decreases (parameters in inverse proportionality corresponding values for BSA; Figure 4B, 4C). The estimated probability of a filament head going into a particular direction is based on 9391 and 12683 measurements of the deflection angles of the filaments heads taken from the movies assigned as Example V (Figure 4A) and Control Assay (Figure 4B), respectively. In the proposed model, a hypothetical filament tip is situated in the middle of a 9-pixel square (Figures 3C, 3D). Taking into account that the pixel size is 100 nm; and that the measured displacement of the filament tip between two consecutive frames is always smaller than 200 nm, an assumption can be made that the head can choose between one of the eight neighboring pixels (Figures 3C, 3D). The frequency counts of the measured deflection angles (Figure 3F) show that the BSA amount and the geometry of BSA pattern on a surface affects directionality of the filament movement.

Several factors can contribute to the motility behavior of actin filaments. First, the uniform gliding of actin filaments on a myosin-coated surface may be disrupted, a feature that was observed before in relation to the actomyosin motility on the patterned surfaces.[69, 70] This may occur due to the low enzymatic activity of the motors,[69] or low concentration of HMM.[21] This uneven motility can manifest in (i) rotation around a fixed point, (ii) formation of a spiral; or (iii)

undulation, similarly to bacterial flagellum.[71] The disruption of motion of cytoskeletal filaments in motility assays was analyzed in details previously.[71] Second, an additional element that influences the nanomechanics of actin filaments is the geometrical distribution of HMM patches on the surface, which modulate the apparent (as opposed to intrinsic) nanomechanical properties of actin filaments. Indeed, the nanopatterning of the surface appears to have an impact not only on the confinement of actin filaments motility, but also on the bending characteristics of actin, which is a semiflexible polymer.[45-51] When the actin filament approaches the boundary between a myosin-rich and BSA-rich areas, the HMM-generated propelling force is transformed into a bending one.[15, 19, 70] The impact of HMM patches on the submicron scale can be quantified through its impact on the apparent persistence length [21] of actin filaments moving on surfaces with different content and geometrical distribution of the ratio of BSA/HMM, as estimated by the level of fluorescent signal in the respective pixels. The persistence length is then understood as the length of a filament over which not only thermal, but also mechanical bending forces become appreciable.[19, 21] The statistical analysis of the actin filaments motility was corroborated with the distribution of the fluorescent signal at the pixel and subpixel resolution level (Figure 5). Visual inspection (Figure 5) suggests that, the larger the area of imprinted surface is, the more frequently the actin filament bends, and consequently its apparent persistence length increases.

C. Shape of the Trajectory of Actin Filaments in Tightly Confined Spaces

The character of the physical interactions between the semiflexible actin polymers and their micro- or nano-environment has been investigated extensively.[47-49, 72-74]

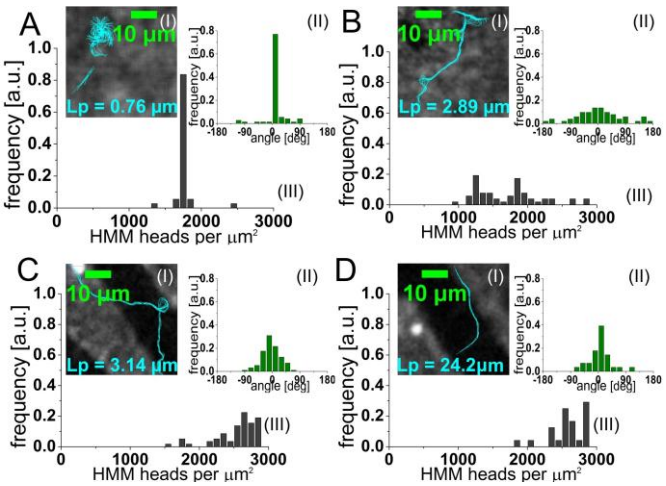

Fig 5. Persistence lengths of actin filaments determined from experimental data. Experimental measurements of averaged end-to-end distance <R> and filament's contours L allowed for determining persistence lengths (Lp) values of chosen filaments. Figures (A), (B), (C), and (D) show distributions of deflection angles correlated both with the HMM concentration (of the pixels visited) and Lp values. Each of the insets presents the overlaid screenshots of the contour of the filament taken from 100 consecutive frames recorded every 0.1s, with the corresponding 8-bit image background.

The semiflexible properties of the actin polymer can be characterized by its persistence length (Figure 2) – a parameter that is defined as the distance above which the movement of the individual parts of the filament becomes uncorrelated.[21, 49]

A number of factors such as confinement, hydrodynamic interactions and flexibility contribute to the significant structural and dynamical fluctuations in the behavior of actin filament.[47-49, 75] Moreover, the geometrical distribution of the motor (HMM), blocking protein (BSA), as well as the ratio between them also influences the actin motility. A simplified assumption is that the filaments should move freely in the HMM-rich areas; and should not enter the BSA-rich ones, thus ensuring the confinement of motility. Therefore the motility of actin filaments, discovered on Leopard skin-like areas that are extremely narrow, tortuous, and with frequent blockages, is a rather unexpected finding. Moreover, the smaller the value of the persistence length, the more the filament bends or buckles (Figure 5: A (I), B (I), C (I), D (I)), which is consistent with the theory and observations made by others.[47-49, 72]

No correlation appears to exist between the length of the actin filament and its persistence length, as also observed by others.[72, 74] Moreover, the analysis of the trajectories shows that the path persistence length directly reflects the filament persistence length (Figure 5: A(I), B(I), C(I), D(I)) as suggested by other studies.[72-74] While some of the findings suggest that the structural features of actin filaments play a minor role in the modulation of motility, other observations come to qualify this conclusion. Intriguingly, it has been observed that if a particular filament is at some point rotating around its head and then continues its movement, there is a high probability that a similar event will repeat along the trajectory of the filament. Conversely, if the filament is moving smoothly, there is a low probability that it will start to rotate around a fixed point. This behavior suggests that the motility of actin filaments is also the consequence of their inherent structure. A possible result of the head denaturation via interaction with surface-immobilized motors was suggested by others,[74] who additionally provided evidence that the changes of this type lead to the increase in bending flexibility of phalloidin-stabilized actin filaments.

The motility characteristics of the actin filaments are modulated by the motors they interact with, either transitory via the HMM surface concentration and activity of the areas visited, with two, one or none heads being active;[69, 72] or more permanently, as alluded before, for the motor-induced conformation changes of the head of filaments. It follows that, by image analysis of the trajectory of the actin filaments, at the highest possible resolution, it is possible to use the standard motility gliding assays [72] to map the information regarding the number of myosin motors present on a surface and their bioactivity state. As the leading head of the actin filament is probing the space ahead, it is critical for events such as rotation, swivelling, or buckling of the filament, described in detail elsewhere.[21, 71, 72]

The results in Figure 5 demonstrate that the amount of HMM (anticorrelated with that of BSA), as well as the

geometry of the HMM pattern, modulate the motility of the actin filament, at the local level: the lower the density of HMM (i.e., higher BSA concentration; and thus the fluorescence intensity of the particular pixel), the higher is the probability that the filament will get trapped and then change original direction of its movement (example in Fig. 5A). Alternatively, regarding global behavior, the smaller the area covered by HMM (the larger the BSA area), the higher the probability of the filaments changing directions rapidly in the population (example in Fig.5B).

The criticality of the interaction of the filament head with the motors stems from several characteristics. First, the actin filament has a polar, anisotropic structure.[21] Second, binding of a protein at the filament tip can trigger structural changes along the filament.[74] From the practical point of view, to be able to harness successfully actin filaments in various types of devices that ask for motility confinement and directionality control, e.g. diagnostic, or biocomputation devices, the persistence length of cytoskeleton filaments should be precisely known and, if possibly, controlled.[72] The values of the persistence length of actin filaments reported in the literature [45, 76, 77] are between 5 and 17 μm, with the latest measurements [73, 78] reporting the value of ~ 8.75 μm. While the average value of 4.67 μm, as calculated here from the motility on narrowly confined spaces, is consistent with the other reports, it is nevertheless placed at the lower end of the spectrum. The practical conclusion from these measurements is that, even in force-wise mild conditions, but size-wise tight, as reported here on BSA/HMM submicron patterns, the apparent low persistence length translates in higher than expected flexibility. Therefore, we predict that the designs of nanodevices aiming to confine and direct the motility of actin filaments will face steeper difficulties that would have been expected from the persistence length estimation based on motility experiments in unconfined geometries.

D. Response of Motility Behavior to Actin Filament Length and HMM Concentration

The fundamental biomechanics of an actomyosin system in a gliding motility assay has been described both conceptually and mathematically in various contributions. The analysis by Duke *et al.*[72] will be used preferentially, albeit not exclusively. Specifically, for the motility assays presented here, we assumed that the HMM molecules are distributed randomly on the nitrocellulose substrate that is free of BSA with a surface concentration that allows the motors reach the filaments isotropically over a distance of ~20 nm.[72] Importantly, HMM heads detached from the filaments for most of their biochemical cycle time,[21, 72] which explains why the filaments can diffuse laterally away after being released by the motor,[72] as reflected in the statistical measurements of velocities and angles discussed further.

The filaments from Example I and III (see Figure 1C for reference) were chosen for scatter plot visualization and analysis. The filaments were labeled, tracked and measured separately through 100 consecutive movie frames. Subsequently, the median value of each parameter was calculated for every separate filament. Both the angle and the velocity values are more scattered for the filaments shorter than 60 nm in comparison with longer filaments (Figure 5 and Figure 6). Also, when actin filaments move on the BSA-free surfaces, i.e., HMM-rich surfaces, the average change of the angle of movement of the filament heads decreases with the filament length (see also Figure 6A in Supporting Information). These length-dependent motility characteristics can be explained by the incapacity of short filaments of reaching the next HMM site after being released by the first one, especially on BSA-rich/HMM-poor regions. Conversely, longer filaments can explore larger areas of the surface to find the motors needed for motility. Indeed, according to the present understanding regarding the actomyosin system,[72] the actin filament is propelled longitudinally only when it is bound to two or more motors. Alternatively, the filament will rotate diffusively,[72] which explains the higher variation in deflection angles for shorter filaments. When the filaments longer than ~1 μm are moving on HMM-rich, but sparse areas, their averaged speed starts to decrease with the length of the filament and this correlation can be approximated by a linear regression (Figure 5, Figure 6 and Supporting Information section). Interestingly, the velocity of the filaments moving on a nitrocellulose surface (without BSA) is approximately constant on the condition that they are longer than ~0.6 μm (see also Figure 7A in Supporting Information). This suggests the presence of additional confinement exerted by BSA patches, but manifested preferentially on longer filaments. Another general observation is that an increase of the deflection angle of the actin filament head corresponds usually to a decreased speed of movement (Figure 5 and Figure 6) in the populations of filaments moving on BSA-imprinted surfaces. The median velocity value of the actin filaments, which is approximately 2 μm/s, as well as the velocity distribution and range, are in agreement with the values

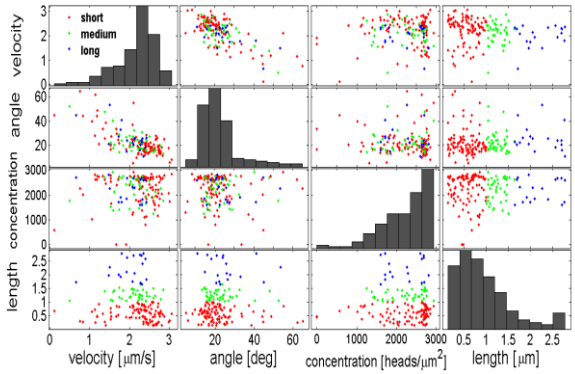

Fig 6. Multi-parameter scatter plot matrix of the parameters characterizing the behavior of actin filaments on the micro-imprinted surface. Each point of the scatter plot matrix represents a central value of the parameter (which is the median value in this case) calculated from 100 different measurements of a particular filament. The filaments are color-coded according to their lengths: red for unusually short (< 1 μm), green for medium (1 ≤ length ≤ 1.5 μm), and blue for long (> 1.5 μm) filaments respectively. (The total number of analyzed filaments is 157).

reported in the literature.[79, 80] However, 2 μm/s is at the lower end of the usually reported range of velocities, which is between 1 and 5 μm/s. This difference may be due to the use of different binning for histograms or using arithmetical means versus medians. The present study used the median, against the averages, for the characterization of the velocities of filaments. As all distributions appeared to be asymmetrical and long-tailed, the arithmetical mean might not reflect the real central value of the population.[54] The median value for deflection angle is approximately 20° in the majority of measured cases, with a significant increase for the population of actin filaments in which the whole motility area is covered with the BSA stamped area (detailed results in Supplementary Information). Nonparametric tests and median values were applied for the statistical characterization of measured parameters as none of the data obtained followed a normal distribution. Similar methods have been used [55] when studying the statistical properties of biological particles.[81]

E. Theoretical Prediction of Actin Behavior based on the Experimental Data

The comprehensive measurements of the key motility parameters of velocity, deflection angle, motor surface concentration, and length of filaments, can be used to predict the behavior of motile actin filaments in future dynamic nanodevices. Furthermore, the HMM surface concentration can be estimated using the fluorescent pixel intensity as a measure of the amount of BSA, which blocks the HMM attachment, following a proper calibration with an independent method, e.g., quartz microbalance, ellipsometry, ATPase assay, although the latter can report values as far as one an order of magnitude lower than those obtained by the former.[72]

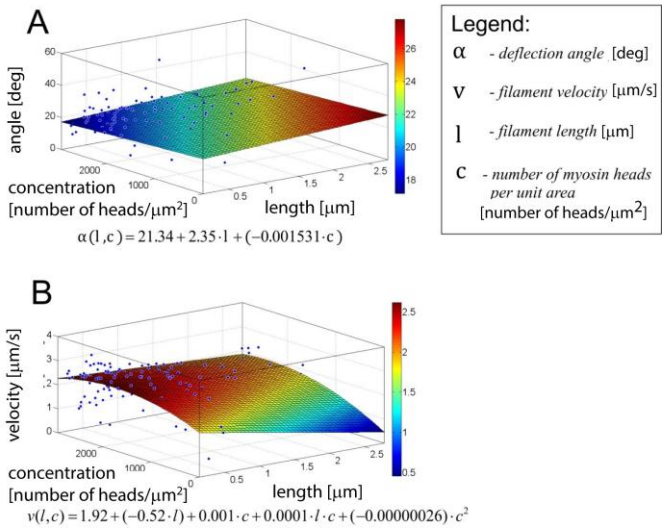

Fig 7. Statistical fit of actin filament motility parameters. We calculated a median value for each parameter. The median values were plotted and used to fit corresponding surfaces with relevant MATLAB toolboxes. The plots A and B show respectively 'deflection angle' and 'velocity' in a function of 'myosin concentration' and 'filament length'. Equations (A) and (B) can be used, especially in the design of dynamic nanodevices, to predict velocity and angular change of the filament having particular length and moving on a surface with particular concentration of myosin motors.

The information from Example I and Example III (see Figure 1C for reference) was used for theoretical prediction of the filament deflection angles (Figure 7A) and velocities (Figure 7B) as a function of both the filament length and approximate myosin concentration on a surface visited by the filament. This was achieved by fitting a surface to the data points (median values) obtained experimentally. Selected 157 filaments were tracked separately through 100 consecutive frames giving ~15700 measurements in total for every single parameter.

The modeling of the velocity and deflection angle as a function of the motor surface density and the filament length would be particularly useful for the design of dynamic nanodevices that use actomyosin system, especially for devices based on the confinement of motility. In such a case, the relationship between the surface concentration of motors and the actin filament length determines the mode of movement and hence directly influences both the directionality and the velocity of the motile objects. Interestingly, Duke *et al.*[72] discriminate three different regimes for the movement of actin filaments, which are remarkably in line with the results reported here. In the first regime, the distances between the motors on a surface are small enough to prevent the filament from bending away from its path more than 20 nm,[72] therefore, the filament follows its contour precisely as it cannot escape the array of myosin heads that have just released it.[72] This corresponds to the situation in which the directional change of the filament head is small, and the velocity is close to the central value of its distribution. In the second regime, when the distances between the motors are considerably higher than above, the filaments can fluctuate between subsequent steps, so they can switch to another motor patch and diffuse.[72] In this case, the filament does not necessarily follow its previous contours, as reflected both in higher deflection angles and more rapid changes of the filament velocities. Finally, in the third regime, below the minimum threshold of the surface concentration, the distances between the motors are so large, that the filament head cannot reach any motor, and it dissociates from the substrate. Thus, the continuous filament movement is disrupted,[72, 73] which can explain the higher variability of the motility parameters for short filaments (<1 μm).

According to the statistical analysis of experimental data, in 75% of all measured cases the deflection angle values are lower than 45°, which is reasonable for the design of the guidance of actin filaments in nanostructures. However, there still exists a low, but noticeable probability of U-turns, even within the BSA-imprinted areas, which can be explained by the high flexibility of actin filaments in comparison with other cytoskeletal filaments, e.g. microtubules.[21, 47-49, 73] More detailed values of measured angles are available in Supporting Information. The possible reasons of U-turns as well as the restriction of turning radius have been discussed and reviewed recently by Nitta *et al.*[73]

IV. Conclusions

Both image and statistical analysis, combined with theoretical reasoning, helped us to provide new insights on the motility behavior of actomyosin on topographically homogenous, but motor-heterogeneous planar systems. Firstly, the filament heads, even when moving within BSA-stamped areas, are following the channels that accidentally adsorbed HMM motors, negotiating the complex network of random and tightly confined spaces. In such cases, the averaged angular change of the filament heads increases compared with the analogue angular values for the BSA-free/HMM-rich surfaces. Furthermore, statistical analysis shows that the behavior of actin filaments is modulated both by their lengths and the surface concentration of motors. Finally, on the basis of experimental results, design-like relationships have been derived for the velocity and deflection angles of the filament heads as a function of the filament lengths and estimated surface concentration.

Acknowledgements

The authors thank Prof. Abe Lee and Lisen Wang at the University of California, Irvine, for providing the master for protein patterning; and to Prof. Cris dos Remedios and Murat Kekic at the University of Sydney for support in protein preparation.

Supporting Information Available

Additional statistical data (Part I of the Supplementary Information) include: frequency counts, box plots, and P-values calculated from permutation tests, as well as histograms with density curves and scatter plots of median values. Analyzed data involves the motility parameters such as velocity, deflection angle, acceleration, and pixel intensity. Detailed information on descriptive statistics of the parameters mentioned above, altogether with comparison of two separated measurement methods, is provided in Part II of the Supplementary Information. Technical information in part III includes: the method of calculation of deflection angles, description of the method used for reading pixel intensity values in MATLAB, equations introducing velocity of the filament movement in function of its length (l) and concentration (c) of myosin heads on the surface, as well as deflection angle in function of length and concentration (l, c).

References

[1] E. Cabezon, V. F. Lanza, and I. Arechaga, "Membrane-associated nanomotors for macromolecular transport," *Current Opinion in Biotechnology*, vol. 23, no. 4, pp. 537-544, 2012.

[2] H. Fukuoka, Y. Inoue, S. Terasawa *et al.*, "Exchange of rotor components in functioning bacterial flagellar motor," *Biochemical and Biophysical Research Communications*, vol. 394, no. 1, pp. 130-135, 2010.

[3] M. G. L. Van Den Heuvel, and C. Dekker, "Motor proteins at work for nanotechnology," *Science*, vol. 317, no. 5836, pp. 333-336, 2007.

[4] M. F. Giraud, P. Paumard, C. Sanchez *et al.*, "Rotor architecture in the yeast and bovine F 1-c-ring complexes of F-ATP synthase," *Journal of Structural Biology*, vol. 177, no. 2, pp. 490-497, 2012.

[5] D. Okuno, R. Iino, and H. Noji, "Rotation and structure of FoF1-ATP synthase," *Journal of Biochemistry*, vol. 149, no. 6, pp. 655-664, 2011.

[6] M. Yoshida, E. Muneyuki, and T. Hisabori, "ATP synthase - A marvellous rotary engine of the cell," *Nature Reviews Molecular Cell Biology*, vol. 2, no. 9, pp. 669-677, 2001.

[7] M. T. Brown, N. J. Delalez, and J. P. Armitage, "Protein dynamics and mechanisms controlling the rotational behaviour of the bacterial flagellar motor," *Current Opinion in Microbiology*, vol. 14, no. 6, pp. 734-740, 2011.

[8] D. Stock, K. Namba, and L. K. Lee, "Nanorotors and self-assembling macromolecular machines: The torque ring of the bacterial flagellar motor," *Current Opinion in Biotechnology*, vol. 23, no. 4, pp. 545-554, 2012.

[9] M. Kikkawa, "The role of microtubules in processive kinesin movement," *Trends in Cell Biology*, vol. 18, no. 3, pp. 128-135, 2008.

[10] A. Yildiz, and P. R. Selvin, "Kinesin: Walking, crawling or sliding along?," *Trends in Cell Biology*, vol. 15, no. 2, pp. 112-120, 2005.

[11] C. Cho, and R. D. Vale, "The mechanism of dynein motility: Insight from crystal structures of the motor domain," *Biochimica et Biophysica Acta - Molecular Cell Research*, vol. 1823, no. 1, pp. 182-191, 2012.

[12] M. J. Bloemink, and M. A. Geeves, "Shaking the myosin family tree: Biochemical kinetics defines four types of myosin motor," *Seminars in Cell and Developmental Biology*, vol. 22, no. 9, pp. 961-967, 2011.

[13] L. M. Coluccio, *Myosins. A Superfamily of Molecular Motors*, Dordrecht, The Netherlands: Springer, 2008.

[14] W. R. Browne, and B. L. Feringa, "Making molecular machines work," *Nature nanotechnology*, vol. 1, no. 1, pp. 25-35, 2006.

[15] S. Diez, J. Helenius, and J. Howard, *Biomolecular motors operating in engineered environments*, p.^pp. 185-199, Weinheim: Wiley-VCH Verlag GmbH & Co., 2004.

[16] F. Fulga, and D. V. Nicolau, "Models of protein linear molecular motors for dynamic nanodevices," *Integrative Biology*, vol. 1, no. 2, pp. 150-169, 2009.

[17] A. Månsson, M. Sundberg, R. Bunk *et al.*, "Actin-based molecular motors for cargo transportation in nanotechnology - Potentials and challenges," *IEEE Transactions on Advanced Packaging*, vol. 28, no. 4, pp. 547-555, 2005.

[18] P. Schwille, and S. Diez, "Synthetic biology of minimal systems synthetic biology of minimal systems P. Schwille and S. Diez," *Critical Reviews in Biochemistry and Molecular Biology*, vol. 44, no. 4, pp. 223-242, 2009.

[19] A. Agarwal, and H. Hess, "Biomolecular motors at the intersection of nanotechnology and polymer science," *Progress in Polymer Science (Oxford)*, vol. 35, no. 1-2, pp. 252-277, 2010.

[20] J. L. Arlett, E. B. Myers, and M. L. Roukes, "Comparative advantages of mechanical biosensors," *Nature nanotechnology*, vol. 6, no. 4, pp. 203-215, 2011.

[21] J. Howard, *Mechanics of motor proteins and the cytoskeleton*: Sinnauer Associates, Inc., 2001.

[22] D. V. Nicolau, D. V. Nicolau Jr, G. Solana *et al.*, "Molecular motors-based micro- and nano-biocomputation devices," *Microelectronic Engineering*, vol. 83, no. 4-9 SPEC. ISS., pp. 1582-1588, 2006.

[23] R. K. Soong, G. D. Bachand, H. P. Neves *et al.*, "Powering an inorganic nanodevice with a biomolecular motor," *Science*, vol. 290, no. 5496, pp. 1555-1558, 2000.

[24] T. Fischer, A. Agarwal, and H. Hess, "A smart dust biosensor powered by kinesin motors," *Nature nanotechnology*, vol. 4, no. 3, pp. 162-166, 2009.

[25] P. Katira, and H. Hess, "Two-stage capture employing active transport enables sensitive and fast biosensors," *Nano Letters*, vol. 10, no. 2, pp. 567-572, 2010.

[26] T. Korten, W. Birnbaum, D. Kuckling *et al.*, "Selective control of gliding microtubule populations," *Nano Letters*, vol. 12, no. 1, pp. 348-353, 2012.

[27] A. Månsson, "Translational actomyosin research: Fundamental insights and applications hand in hand," *Journal of Muscle Research and Cell Motility*, vol. 33, no. 3-4, pp. 219-233, 2012.

[28] A. Månsson, R. Bunk, M. Sundberg *et al.*, "Self-organization of motor-propelled cytoskeletal filaments at topographically defined

borders," *Journal of Biomedicine and Biotechnology*, vol. 2012, 2012.

[29] E. N. Vasina, E. Paszek, D. V. Nicolau Jr *et al.*, "The BAD project: Data mining, database and prediction of protein adsorption on surfaces," *Lab on a Chip - Miniaturisation for Chemistry and Biology*, vol. 9, no. 7, pp. 891-900, 2009.

[30] E. P. Ivanova, J. P. Wright, D. Pham *et al.*, "Polymer microstructures fabricated via laser ablation used for multianalyte protein microassay," *Langmuir*, vol. 18, no. 24, pp. 9539-9546, 2002.

[31] D. V. Nicolau, T. Taguchi, H. Taniguchi *et al.*, "Micron-sized protein patterning on diazonaphthoquinone/novolak thin polymeric films," *Langmuir*, vol. 14, no. 7, pp. 1927-1936, 1998.

[32] D. V. Nicolau, T. Taguchi, H. Taniguchi *et al.*, "Negative and positive tone protein patterning on e-beam/deep-UV resists," *Langmuir*, vol. 15, no. 11, pp. 3845-3851, 1999.

[33] J. Wright, E. Ivanova, D. Pham *et al.*, "Positive and negative tone protein patterning on a photobase generating polymer," *Langmuir*, vol. 19, no. 2, pp. 446-452, 2003.

[34] Y. Xia, and G. M. Whitesides, "Soft lithography," *Angewandte Chemie - International Edition*, vol. 37, no. 5, pp. 550-575, 1998.

[35] M. B. Kolli, B. S. Day, H. Takatsuki *et al.*, "Application of poly(amidoamine) dendrimers for use in bionanomotor systems," *Langmuir*, vol. 26, no. 9, pp. 6079-6082, 2010.

[36] D. J. G. Bakewell, and D. V. Nicolau, "Protein linear molecular motor-powered nanodevices," *Australian Journal of Chemistry*, vol. 60, no. 5, pp. 314-332, 2007.

[37] M. Lard, L. Ten Siethoff, J. Generosi *et al.*, "Molecular motor transport through hollow nanowires," *Nano Letters*, vol. 14, no. 6, pp. 3041-3046, 2014.

[38] J. A. Barden, and C. G. Dos Remedios, "The environment of the high-affinity cation binding site on actin and the separation between cation and ATP sites as revealed by proton NMR and fluorescence spectroscopy," *Journal of Biochemistry*, vol. 96, no. 3, pp. 913-921, 1984.

[39] M. E. Carsten, and W. F. Mommaerts, "A study of actin by means of starch gel electrophoresis," *Biochemistry*, vol. 2, pp. 28-32, 1963.

[40] S. S. Margossian, and S. Lowey, "[7] Preparation of myosin and its subfragments from rabbit skeletal muscle," *Methods in Enzymology*, 1982, pp. 55-71.

[41] J. A. Spudich, and S. Watt, "The regulation of rabbit skeletal muscle contraction. I. Biochemical studies of the interaction of the tropomyosin-troponin complex with actin and the proteolytic fragments of myosin," *Journal of Biological Chemistry*, vol. 246, no. 15, pp. 4866-4871, 1971.

[42] L. Ceriotti, N. F. De Rooij, and E. Verpoorte, "An integrated fritless column for on-chip capillary electrochromatography with conventional stationary phases," *Analytical Chemistry*, vol. 74, no. 3, pp. 639-647, 2002.

[43] D. C. Duffy, J. C. McDonald, O. J. A. Schueller *et al.*, "Rapid prototyping of microfluidic systems in poly(dimethylsiloxane)," *Analytical Chemistry*, vol. 70, no. 23, pp. 4974-4984, 1998.

[44] J. R. Sellers, G. Cuda, F. Wang *et al.*, "Myosin-specific adaptations of the motility assay," *Methods in cell biology*, vol. 39, pp. 23-49, 1993.

[45] F. Gittes, B. Mickey, J. Nettleton *et al.*, "Flexural rigidity of microtubules and actin filaments measured from thermal fluctuations in shape," *Journal of Cell Biology*, vol. 120, no. 4, pp. 923-934, 1993.

[46] J. Käs, H. Strey, J. X. Tang *et al.*, "F-actin, a model polymer for semiflexible chains in dilute, semidilute, and liquid crystalline solutions," *Biophysical Journal*, vol. 70, no. 2 I, pp. 609-625, 1996.

[47] S. Köster, J. Kierfeld, and T. Pfohl, "Characterization of single semiflexible filaments under geometric constraints," *European Physical Journal E*, vol. 25, no. 4, pp. 439-449, 2008.

[48] S. Köster, and T. Pfohl, "An in vitro model system for cytoskeletal confinement," *Cell Motility and the Cytoskeleton*, vol. 66, no. 10, pp. 771-776, 2009.

[49] S. Köster, D. Steinhauser, and T. Pfohl, "Brownian motion of actin filaments in confining microchannels," *Journal of Physics Condensed Matter*, vol. 17, no. 49, pp. S4091-S4104, 2005.

[50] A. Ott, M. Magnasco, A. Simon *et al.*, "Measurement of the persistence length of polymerized actin using fluorescence microscopy," *Physical Review E*, vol. 48, no. 3, pp. R1642-R1645, 1993.

[51] S. Trachtenberg, Hammel, H., "Determining the persistence length of biopolymers and rod-like macromolecular assemblies from electron microscope images and deriving some of their mechanical properties," *Microscopy: Science, Technology, Applications and Education*, pp. 1690-1695, 2010.

[52] H. Nagashima, and S. Asakura, "Dark-field light microscopic study of the flexibility of F-actin complexes," *Journal of Molecular Biology*, vol. 136, no. 2, pp. 169-182, 1980.

[53] D. G. Altman, *Practical Statistics for Medical Research*, London: Chapman & Hall, 1991.

[54] D. S. Moore, McCabe, G. P., Craig, B. A., *Introduction to the Practice of Statistics*, New York: W. H. Freeman and Company, 2012.

[55] B. Vidakovic, "Statistics for Bioengineering Sciences with MATLAB and WinBUGS Support," Springer New York Dordrecht Heidelberg London, 2011.

[56] R. C. Gonzalez, Woods, R. E., *Digital Image Processing using MATLAB*, USA: Gatesmark, LLC, 2009.

[57] C. Fink, F. Morgan, and L. M. Loew, "Intracellular fluorescent probe concentrations by confocal microscopy," *Biophysical Journal*, vol. 75, no. 4, pp. 1648-1658, 1998.

[58] Y. Hanaoka, I. Suzuki, and T. Sakurai, "Practical method to derive nonlinear response functions of cameras for scientific imaging," *Applied Optics*, vol. 50, no. 16, pp. 2401-2407, 2011.

[59] R. L. Lakowicz, *Principles of Fluorescence Spectroscopy. Third Edition*, University of Maryland School of Medicine, Baltimore, USA: Springer, 2006.

[60] Z. Pang, N. E. Laplante, and R. J. Filkins, "Dark pixel intensity determination and its applications in normalizing different exposure time and autofluorescence removal," *Journal of Microscopy*, vol. 246, no. 1, pp. 1-10, 2012.

[61] J. C. Russ, *The Image Processing Handbook. 6th Edition.*, 2011.

[62] W. K. Wan, M. A. Lovich, C. W. Hwang *et al.*, "Measurement of drug distribution in vascular tissue using quantitative fluorescence microscopy," *Journal of Pharmaceutical Sciences*, vol. 88, no. 8, pp. 822-829, 1999.

[63] J. C. Waters, "Accuracy and precision in quantitative fluorescence microscopy," *Journal of Cell Biology*, vol. 185, no. 7, pp. 1135-1148, 2009.

[64] R. A. Carmona, *Statistical Analysis of Financial Data in S-Plus*, p.^pp. 14-23, Department of Statistics, University of Princeton, USA: Springer, 2004.

[65] Y. Xia, and G. M. Whitesides, *Self-assembled Monolayer Films: Microcontact Printing*: Elsevier Ltd, 2001.

[66] A. Bernard, E. Delamarche, H. Schmid *et al.*, "Printing patterns of proteins," *Langmuir*, vol. 14, no. 9, pp. 2225-2229, 1998.

[67] J. D. Crenshaw, T. Liang, H. Hess *et al.*, "A cellular automaton approach to the simulation of active self-assembly of kinesin-powered molecular shuttles," *Journal of Computational and Theoretical Nanoscience*, vol. 8, no. 10, pp. 1999-2005, 2011.

[68] F. Fulga, and D. V. Nicolau, "Optimum time and space resolution for tracking motile nano-objects."

[69] D. V. Nicolau, G. Solana, M. Kekic *et al.*, "Surface hydrophobicity modulates the operation of actomyosin-based dynamic nanodevices," *Langmuir*, vol. 23, no. 21, pp. 10846-10854, 2007.

[70] D. V. Nicolau, H. Suzuki, S. Mashiko *et al.*, "Actin motion on microlithographically functionalized myosin surfaces and tracks," *Biophysical Journal*, vol. 77, no. 2, pp. 1126-1134, 1999.

[71] L. Bourdieu, T. Duke, M. B. Elowitz *et al.*, "Spiral defects in motility assays: A measure of motor protein force," *Physical Review Letters*, vol. 75, no. 1, pp. 176-179, 1995.

[72] T. Duke, T. E. Holy, and S. Leibler, ""Gliding assays" for motor proteins: A theoretical analysis," *Physical Review Letters*, vol. 74, no. 2, pp. 330-333, 1995.

[73] T. Nitta, A. Tanahashi, Y. Obara *et al.*, "Comparing guiding track requirements for myosin-and kinesin-powered molecular shuttles," *Nano Letters*, vol. 8, no. 8, pp. 2305-2309, 2008.

[74] P. G. Vikhorev, N. N. Vikhoreva, and A. Månsson, "Bending flexibility of actin filaments during motor-induced sliding," *Biophysical Journal*, vol. 95, no. 12, pp. 5809-5819, 2008.

[75] R. Chelakkot, R. G. Winkler, and G. Gompper, "Semiflexible polymer conformation, distribution and migration in

microcapillary flows," *Journal of Physics Condensed Matter*, vol. 23, no. 18, 2011.

[76] D. Riveline, C. H. Wiggins, R. E. Goldstein *et al.*, "Elastohydrodynamic study of actin filaments using fluorescence microscopy," *Physical Review E - Statistical Physics, Plasmas, Fluids, and Related Interdisciplinary Topics*, vol. 56, no. 2, pp. R1330-R1333, 1997.

[77] T. Yanagida, M. Nakase, K. Nishiyama *et al.*, "Direct observation of motion of single F-actin filaments in the presence of myosin," *Nature*, vol. 307, no. 5946, pp. 58-60, 1984.

[78] X. Liu, and G. H. Pollack, "Mechanics of F-actin characterized with microfabricated cantilevers," *Biophysical Journal*, vol. 83, no. 5, pp. 2705-2715, 2002.

[79] A. Månsson, and S. Tågerud, "Multivariate statistics in analysis of data from the in vitro motility assay," *Analytical Biochemistry*, vol. 314, no. 2, pp. 281-293, 2003.

[80] N. N. Vikhoreva, P. G. Vikhorev, M. A. Fedorova *et al.*, "The in vitro motility assay parameters of actin filaments from Mytilus edulis exposed in vivo to copper ions," *Archives of Biochemistry and Biophysics*, vol. 491, no. 1-2, pp. 32-38, 2009.

[81] A. Matov, K. Applegate, P. Kumar *et al.*, "Analysis of microtubule dynamic instability using a plus-end growth marker," *Nature Methods*, vol. 7, no. 9, pp. 761-768, 2010.